ANL-78-23

PHYSICS OF REACTOR SAFETY

Quarterly Report

October–December 1977

ARGONNE NATIONAL LABORATORY, ARGONNE, ILLINOIS

Prepared for the U. S. NUCLEAR REGULATORY COMMISSION
under Contract W-31-109-Eng-38

Printed in the United States of America
Available from
National Technical Information Service
U. S. Department of Commerce
5285 Port Royal Road
Springfield, Virginia 22161
Price: Printed Copy $4.50; Microfiche $3.00

Distribution Category:
Advanced Reactor Safety
Research—Fast Reactors
(NRC-7)

ANL-78-23

ARGONNE NATIONAL LABORATORY
9700 South Cass Avenue
Argonne, Illinois 60439

PHYSICS OF REACTOR SAFETY

Quarterly Report
October—December 1977

Applied Physics Division

March 1978

Work performed for the
Division of Reactor Safety Research
U. S. Nuclear Regulatory Commission

Previous reports in this series

ANL-77-22	October—December 1976
ANL-77-48	January—March 1977
ANL-77-69	April—June 1977
ANL-77-92	July—September 1977

TABLE OF CONTENTS

TABLE OF CONTENTS

LIST OF FIGURES

LIST OF TABLES

PHYSICS OF REACTOR SAFETY

Quarterly Report
October-December 1977

ABSTRACT

This quarterly progress report summarizes work done in Argonne National Laboratory's Applied Physics Division and Components Technology Division for the Division of Reactor Safety Research of the U. S. Nuclear Regulatory Commission during the months of October-December 1977. The work in the Applied Physics Division includes reports on reactor safety program by members of the Reactor Safety Appraisals Group, Monte Carlo analysis of safety-related critical assembly experiments by members of the Theoretical Fast Reactor Physics Group, and Planning of Safety-Related (ZPR) Planning and Experiments Group. Work on reactor core thermal-hydraulic code development performed in the Components Technology Division is also included in this report.

I. TECHNICAL COORDINATION - FAST REACTOR SAFETY ANALYSIS (A2015)

A. Summary

The generalized version of POOLVENS was completed with several additional improvements made.

Study using FX2-POOL of the Behrens effect in pools with recompaction indicate that a significant portion of the pool surface area must be coherently pressurized to give a significant energy deposition.

The LASL KFIX code has been implemented. The significance of the improvements in its hydrodynamics methods over those of KACHINA will be evaluated.

The effect of a residual sodium film in the fission gas plenum region (assumed to be above the core) after sodium voiding on mechanical energy yield in a LOF accident in an LMFBR is being evaluated. If heat transfer is assumed to be equal to that corresponding to the condensation of pure fuel vapor on steel, the sodium film would be heated to boiling in about 20 ms. If a sodium vapor film is then assumed produced, heat transfer from the fuel vapor is greatly reduced and it would require a number of seconds to vaporize the film completely. However, entrainment of sodium droplets could considerably enhance the rate of fuel-sodium heat transfer and the consequent rise in sodium vapor pressure.

Several new features have been added to EPIC, including axial growth of the molten fuel cavity during a transient.

A number of areas in fuel pin mechanics have been reviewed, including the modeling used in the FPIN code being developed by the RAS Division of ANL, and data on fission gas retention and transient release. The FRESS code has been modified to make possible analysis of TREAT experiments. The HEDL COBRA-3M code has been implemented to calculate temperatures for FRESS. The E-8 and H-6 TOP experiments are being analyzed with this code.

B. Study of Basic Problems in Accident Analysis

1. FX2-POOL Development (P. B. Abramson)

The generalized version of POOLVENS was completed including the following features.

a) Variable number of DPIC (distributed-particle-in-cell) particles (suggested 4 per 2D cell)
b) Optional stochastic treatment of heat transfer user input mean and signs for drop size and effective heat transfer coefficient
c) Variable mesh
d) Color/black and white/none movie plots
e) Variable storage selection

2. Behrens Effect (P. B. Abramson)

Further studies of recompaction in pools using FX2-POOL were carried out in connection with comparable work with VENUS by E. L. Fuller of EPRI. Our work indicates that a significant portion of the surface area of a pool must be coherently pressurized in order to cause any significant energy deposition (starting from a "bare" pool at prompt critical). Work will now be directed at initially subcritical pools with material relocated axially and radially away from the pool.

3. FX2-TWOPOOL (J. J. Sienicki)

A copy of the KFIX code was obtained from J. R. Travis (LASL). KFIX is a two-phase, two-field thermohydrodynamics code for one material in two dimensions which implicitly includes interphase exchange within the ICE multifield methodology. The CDC version received has been converted to IBM and implemented on the ANL 370/195 and has successfully executed a sample problem. We shall compare the thermohydrodynamic methods of TWOPOOL with those of KFIX and we shall also assess the capabilities of the KFIX methods to determine what improvement they offer over those of KACHINA for SIMMER applications.

4. Role of Sodium Films in Accident Energetics (P. L. Garner and P. B. Abramson)

A recent series of SIMMER calculations[1] has indicated that the system kinetic energy associated with the post-disassembly core expansion following a LOF may be significantly reduced by deterministically treating the numerous phenomena involved. These calculations assumed that the fission-gas-plenum region, in addition to the core and upper axial blanket, was completely voided of sodium. Experiments[2] have shown that a liquid film, comprising 15 to 20% of the channel flow area, is left on the channel walls following an expulsion event. A complete treatment of this sodium film might have a significant impact on the recent "vessel problem" calculations performed using SIMMER. A study of phenomena associated with the sodium film has been initiated, and some initial results are reported here.

Previous work[3] has indicated that the vaporization of a small amount of liquid sodium following its entrainment into an expanding two-phase liquid/vapor fuel region can increase the system expansion work to a value higher than that due to fuel expansion alone; entrainment of large amounts of liquid sodium into the expanding mixture will simply quench the fuel and decrease the expansion work to a value below that due to fuel expansion alone. The actual process of vaporizing the sodium film can inhibit the loss of energy from the expanding core region to the structure by fuel condensation thus leaving a sizeable amount of energy still available in the fuel to be converted to system kinetic energy.

An initial set of calculations has been performed assuming that the heat flux available for sodium film vaporization may be approximated by the heat flux[4] associated with pure fuel vapor condensing onto solid steel (which melts). This heat flux is used to supply both sensible heat and latent heat of vaporization for the sodium as well as to provide a sensible heating of the underlying cladding. The latter effect was included since a transient conduction heat transfer calculation showed that the cladding and liquid sodium

film rise rather uniformly in temperature when subjected to the heating rate associated with fuel condensation onto steel. A 0.15 mm thick sodium film (corresponding to 20% of the channel flow area) can be raised to its boiling temperature (at 0.1 MPa) in approximately 20 ms and be completely vaporized in 100 to 150 ms under these assumptions. If higher heating rates are used, the sodium/fuel interface temperature can rise much faster and the time to cut off fuel condensation could be reduced by as much as an order of magnitude.

The actual process of producing sodium vapor could alter the fuel condensation rate — an effect which was neglected in the calculations stated in the previous paragraph. Several calculations have been performed to estimate the magnitude of this feedback. These calculations used the models in Reference 4 but replaced the steel solid and liquid regions with sodium liquid and vapor, respectively. The calculational procedure thus assumed that the sodium vapor produced exists as a discrete layer separating the condensed fuel from the liquid soidum film. The calculated results indicated that the fuel condensation rate is decreased by two orders of magnitude by the production of sodium vapor and the complete film vaporization times are correspondingly increased to the order of seconds. (Sodium vaporization begins immediately following contact between the fuel and soidum in these calculations.) The fuel condensation rate reduction reported here is similar to that reported by Suo-Antilla[5] although quite different models have been used in the two calculations.

These initial calculations provide indications of the mass and energy fluxes associated with a fuel-condensation/sodium-vaporization situation. This information will be integrated into a model being developed for analyzing the transient pressurization and system kinetic energy alterations associated with sodium film vaporization. These future calculations must be performed in order to assess the importance of properly treating the sodium film in accident analysis calculations.

The "real" problem will be dynamic (hydrodynamically) rather than static, and issues of the hydrodynamic interactions between the streaming and condensing fuel vapor and two phase fuel/steel mixture will eventually have to be included in assessing the actual pressure-time history at the lower interface of the sodium "slug". These preliminary calculations indicate that even in the static case the fuel vapor pressure reduction by condensation would be cut off in a time scale of about 20 ms and after that sodium pressures could be contributing. One might expect the dynamic effects of tearing sodium droplets off of the film and entraining them into the flowing two phase mixture to cause relatively rapid rises in sodium pressurizations.

5. EPIC Code Development (P. A. Pizzica and P. L. Garner)

The fuel-pin cavity melt-in model and the time-dependent cladding-breach-size option in the EPIC code have been modified. The molten fuel cavity in the pin may now grow axially (radial growth was included previously) as the energy deposition causes the additional segments to become molten. An option has been included in the code to allow the cladding breach to lengthen axially in time as the fuel pin cavity reaches a user-specified radial melt fraction at each axial node.

EPIC results may now be displayed as a color movie. The movie displays the growth of the FCI zone, sodium slug expulsion, growth of the molten fuel

cavity in the pin, motion of fuel in the pin and channel, and fuel temperatures as the calculation proceeds.

6. Fuel Pin Mechanics Studies (Kalimullah)

a) A review of a description (ANL/RAS 77-23) of the FPIN pin failure program shows the following important features of the program:

i) The outer cracked fuel is modeled as a large number of elastic props laid radially between the cladding and the continuous viscoelastic fuel. The circumferential and axial stresses in these props equal the negative of the pressure of the gas in the cracks. This model gives an upper limit of the force transmitted to the clad because some slippage among and crushing of cracked pieces will occur.

ii) A sensitive parameter used in modeling the continuous visco-elastic fuel is the equivalent creep strain rate of the fuel as a function of equivalent stress, fuel temperature and equivalent plastic strain - little studied for fuel.

iii) The central cavity model seems reasonable but the calculation of the amount of gas in the cavity is not complete.

iv) The clad stress and strain calculation is reasonable but a failure criterion has not been added.

v) No gas is released before melting and all gas is released at the instant of melting.

b) The percolation theory model used in the GRASS code (being developed at ANL) and the LANGZEIT code (Karlsruhe) for fission gas release from grain boundaries to outside of a pellet piece was reviewed and found unsuitable for use in a transient overpower situation.

c) Both the FGR series tests at HEDL and the DEH tests at ANL for studying fission gas release and fuel behavior during TOP have similar conclusions. Fuel breaks up due to fission gas at outer radii to pieces almost of the size of grains for heating rates greater than about 300°K/sec (ANL-RDP-61, pp. 4.2-7).

d) A capability of analyzing one specified pin of a multipin test subassembly has been added to the FRESS program for fuel pin failure so that TOP experiments performed in TREAT may be analyzed. Some other additions to this program include calculations of the average gas pressure of the molten nodes, average gas pressure of the whole pin, etc.

e) Review of experimental data on fission gas retention shows that (a) a saturation amount of retained fission gas ($\sim 0.12 \times 10^{20}$ atoms/cm length of a typical LMFBR pin at 15 kW/ft linear power) is reached at 5 to 5.5 a/o burnup; the saturation amount is twice this value at 10 kW/ft and thrice at 5 kW/ft; (b) for burnups as low as 2 to 3 a/o the gas retained in 0.1 to

1 μm bubbles, almost all at grain boundaries, is 1 to 4 times that inside grains in atomic solution or smaller bubbles.[6]

(f) We are planning to use the FRESS code for parametric studies of pin clad failure by fission gas loading and for analysis of TREAT experiments. FRESS is linked to COBRA-3M, which supplies fuel temperatures corresponding to an input reactor power history. Application of the FRESS fuel pin failure program to E-8 and H-6 TOP tests in TREAT results in slightly late failure predictions but this result is obscured by significant errors found in the COBRA code. Since the various modifications of COBRA-3M modified at ANL to account for fuel pin melting were found to have serious errors, the version of COBRA-3M improved at HEDL to include pin melting has been obtained and an input for the E-8 TREAT test is being prepared. The code will be used to write a dataset containing the radial and axial temperature distribution in fuel, cladding and coolant for input to FRESS.

7. 2000 MWe Mixed Oxide LMFBR Power and Reactivity Distribution (Kalimullah, P. A. Pizzica and H. H. Hummel)

Power and reactivity distributions in a 2000 MWe mixed oxide LMFBR at BOEC have been computed for input to the SAS3D/EPIC code to study LOF-driven TOP accidents. Nine channels have been chosen to represent the three burnup stages. It is not currently feasible to use more than twelve or thirteen channels with SAS/EPIC because of computer storage limitations.

C. Coordination of RSR Fast Reactor Safety Research

P. B. Abramson and J. J. Sienicki met with J. Travis (LASL) to discuss numerical hydrodynamics methodology and to obtain information on KFIX for comparison with TWOPOOL. P. B. Abramson and J. J. Sienicki also met with M. Stevenson, J. Jackson, R. Alcouffe and R. Henninger to discuss SIMMER validation on October 26.

P. L. Garner attended a meeting of the properties and modeling subgroup of the Aerosol Release and Transport Review Group in Silver Spring on October 27, 1977.

P. B. Abramson met with C. Kelber, R. Curtis, M. Silberberg, D. Basdekas and P. Wood at Silver Spring on November 14 to discuss SIMMER experimental support.

P. B. Abramson and E. M. Gelbard met with E. Vaughn (AI) and T. Hoffman (ORNL) on November 31 to discuss the future needs in Behrens effect studies.

P. B. Abramson met with J. Walker, W. Camp and M. Stevenson on December 1 to discuss coordination of analysis of in-pile experiments.

P. B. Abramson met with R. Coats and S. Eisenhower at SANDIA on December 19 to discuss coordination of experiments for SIMMER verification and to review films of the fuel dispersal test.

Work is under way on comparative accident calculations being conducted by the EEC Whole Core Accident (WAC) Committee. Both an LOF and a TOP case are being considered. It is anticipated that results of the LOF case will be

published in the spring of 1978 and results of the TOP case in the fall of 1978.

A bilateral program in accident analysis involving the UKAEA and the USNRC is being formulated. It is expected that work on this program will begin early in 1978.

PUBLICATIONS

1. "Bubble Collapse Reactivity Increases in Boiling Fuel/Steel Pools," P. B. Abramson, T. A. Daly, R. Lell and E. M. Gelbard, TANSAO 27, (November 1977).

2. "Stochastically Variable Parameters in Probabilistic Accident Analysis," P. B. Abramson, H. H. Hummel, E. M. Gelbard, P. A. Pizzica and J. J. Sienicki, TANSAO 27 (November 1977).

3. "On the System Damage Potential for CRBRP," J. J. Hakim, P. B. Abramson and R. J. Henninger, TANSAO 27 (November 1977).

II. MONTE CARLO ANALYSIS AND CRITICALS PROGRAM PLANNING FOR SAFETY-RELATED CRITICALS (A2018)

A. Monte Carlo Analysis of Safety-Related Criticals (E. M. Gelbard)

The high degree of complexity inherent in modeling a complete heterogeneous assembly dictates that the preparation of input data be automated wherever possible. The main effort in the latter part of 1977 was directed toward gathering detailed information on all materials used in the RSR experiments. This information consists of the geometry, mass and composition of every component used in the assembly. The latter, together with drawer master and loading matrix information, is synthesized and translated into a data format suitable for input into the VIM code. Data synthesis and translation is accomplished with two utility codes that have been written for this purpose.

1) DTMTX: The DTMTX code reads cards produced from the final core loading (5000 drawers in the RSR reference core) and produces a unique set of drawer types (13 drawer types in the RSR reference core). The drawer types, along with their location in the assembly matrix, are in VIM input format.

2) VIP: The VIP code takes all the remaining information and produces the geometry and number density data in VIM input format.

Both codes have been designed to utilize the nomenclature and conventions presently in use in the experimental area and it is hoped that they are sufficiently general to allow future use in other experimental analysis.

The DTMTX phase has been completed for the reference core. All structural materials (matrix tubes, drawers, sprongs and shirns) have been coded and are ready to process through VIP. Approximately 75% of the plates have been coded are ready for processing.

One feature of the VIP code, that results in a substantial reduction of duplicated effort, is the use of a material library. Once a material (matrix tube, drawer, plate etc.) is entered in the VIP library, that material need not be coded again. Thus, in creating the library for the reference core, a majority of the data reduction and synthesis has also been done for subsequent steps in the meltdown sequence.

B. Planning of Demo Safety Related Experiments (S. K. Bhattacharyya and L. LeSage)

The Demo Safety Related Critical Experiments program was completed, on schedule, on December 30, 1977. The original program plans consisted of measurements in axially symmetric accident configurations.[7] Two of the original six configurations (viz. the axially symmetric blanket collapse and the symmetric fuel slump-out into axial blanket) were assigned a low priority during the program planning stage with the idea that if time pressures so dictated they would be eliminated from the program. During the experimental program it was found necessary to eliminate the configurations because of the operational reasons described below.

The fuel slump-out in axial blanket configuration would result in a calculated eigenvalue of 0.90. Such large subcriticalities cannot be measured accurately (to within 20%) with the available noise techniques. In addition, since the planned physics program would have to be performed in a critical configuration, a very large number of edge drawers (estimated to be 200) would have to be added. The expected results did not appear to be of sufficient interest to warrant making such large loading changes. These considerations eliminated this configuration.

The axially symmetric blanket collapse configuration had a calculated reactivity addition of 2% $\Delta k/k$ relative to the axially symmetric fuel slump-in configuration.[7] This reactivity would be compensated by the replacement of core edge drawers with radial blanket drawers. Since the operational control rods were located at the core/radial blanket boundary for the slump-in case, it would be impossible to achieve a critical configuration with the blanket-collapse condition without causing some of the rod locations to be in the blanket and thereby losing the necessary 2% Δk in control rods. Thus, this configuration was also eliminated from the program.

A modified plan for the remainder of the program, was designed to avoid these difficulties while keeping to the basic philosophical frame-work outlined in Ref. 7. Axially asymmetric fuel slump-in and fuel slump-out configurations were proposed for the remainder of the time available to the program. In addition, an axially asymmetric fuel slump-in with blanket collapse configuration was also proposed. A layout of the final configurations in the program is shown in Fig. 1. Table I summarizes the measurements undertaken in these configurations.

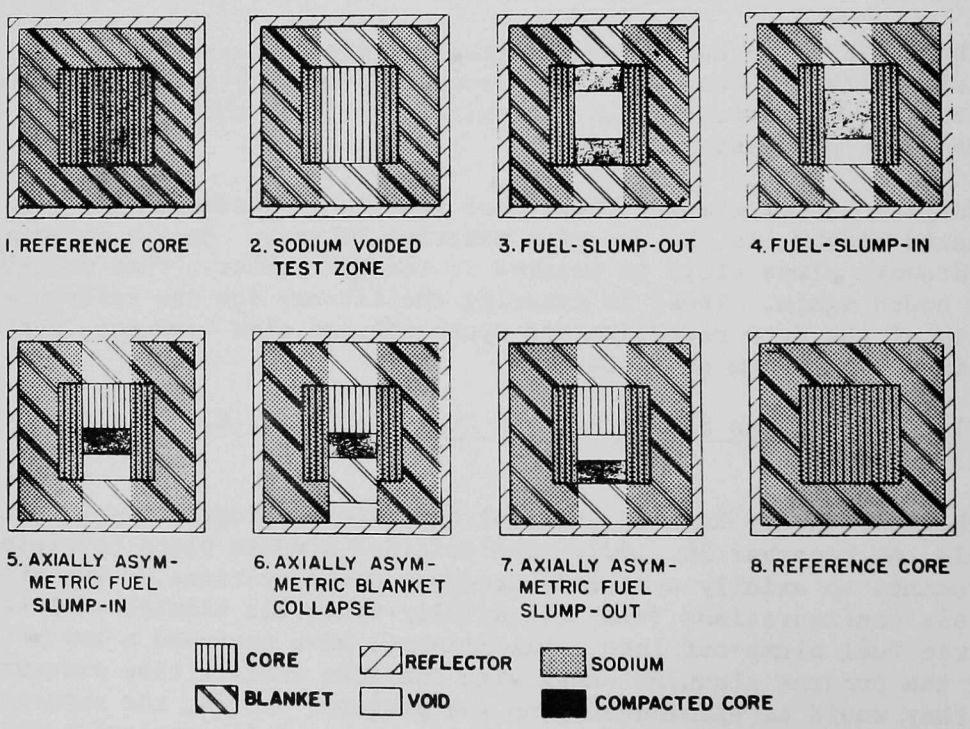

Fig. 1. Layout of the Configurations for the Safety Related Critical Experiments. ANL-116-78-126

TABLE I. Measurements to be Performed in the Axially Asymmetric Meltdown Configurations

Configuration	Δk [Configuration Worth]	Reaction Rate Traverse $^{235}U(n,f)$ (Axial)	Reactivity Worth Traverse (Axial) ^{239}Pu Stainless Steel	^{241}Pu Decay Worth
1. Axially asymmetric slump-in	✓	✓	✓	
2. Axially asymmetric slump-in[a] with blanket collapse	✓			
3. Axially asymmetric slump-out	✓	✓	✓	
4. Sodium filled reference				✓

[a]This configuration has been assigned a low priority and will be eliminated if time pressures so dictate.

The primary rationale for going to the axially asymmetric configurations was to avoid, for operational reasons, the large reactivity changes associated with axially symmetric loadings. An additional consideration was the fact that axially asymmetric fuel compaction events are of high interest to safety analysts. With the revised plan, fuel slump-in and slump-out measurements are available for both the axially symmetric and axially asymmetric conditions; a comparison of the two should yield valuable insight into the calculational difficulties with axially asymmetric configurations. (Some axially asymmetric measurements were planned for the BIZET-B program at Winfrith,[8] but the program has been cancelled). The deviation from the originally planned program is very small from an operational point of view.

Experimental Results

During the course of the program, the reactivity worth of the configuration changes were determined and various integral neutronic parameters were measured in several of the configurations. The large volume of data accumulated during the program are presently being analyzed. Some preliminary results are reported here.

1. Configuration Worths

Table II lists the preliminary experimental worths of the axially symmetric and asymmetric configurations. These numbers are preliminary because the kinetics parameters used to analyze the experimental data were preliminary. The results are presented here to show the trends and approximate magnitude of reactivity worths. The partial slump configurations were achieved by loading three columns of fuel in the slumped region (instead of four) and the large negative worth reflects the effects of this net loss of fuel. It is of interest to note that the axially symmetric fuel slump-out involves a small incremental change in negative worth from the asymmetric slump-out case. In contrast, the axially symmetric fuel slump-in case involves a very large incremental change in positive worth from the asymmetric case. The preanalysis overpredicted the negative worth of fuel slump-out and underpredicted the worth of fuel slump-in. The preanalysis results, however, are known to be inaccurate because of the use of homogeneous cross-sections.

TABLE II. Preliminary Reactivity Worths for the Various Configuration Changes During the Demo Safety Related Critical Experiment Program

Configuration	Preliminary Worth[a] (Ih)[b]
1. Axially Asymmetric Fuel Slump-Out	-516 ± 6
2. Axially Symmetric Partial Fuel Slump-Out[c]	-5117 ± 329
3. Axially Symmetric Fuel Slump-Out	-780 ± 13
4. Axially Asymmetric Fuel Slump-In	+655 ± 23
5. Axially Symmetric Partial Fuel Slump-In[c]	-4766 ± 280
6. Axially Symmetric Fuel Slump-In	+2106 ± 57
7. Axially Asymmetric Fuel Slump-In with Blanket Collapse	+1218 ± 14

[a] All the worths are relative to the axially symmetric sodium-voided test zone configurations worth.

[b] 1% $\Delta k/k$ = 976 Ih.

[c] These configurations had less fuel in the test zone than the reference configurations because of the way the partial slump configurations were designed. The other configurations all had the same amount of fuel as the reference configuration.

2. Fission Rate Distribution

Figure 2 shows a layout of the reference core. The fission rate distribution of ^{235}U was determined both radially and axially in the core using enriched uranium foils. For comparison with Monte Carlo calculations, the foils were arranged in planar arrays at different radial locations to simulate large planar foils. Table III gives the radial fission distribution in the core (see Fig. 2 for identification of the locations of these foils). In the radial space spanned, the fission rate drops off by a factor greater than 3. Table IV gives the axial fission rate distribution, the value of Z being measured from the axial midplane. The axial fission rate drops off by almost a factor of 5. A comparison of these experimental results with Monte Carlo and conventional calculations will be of great interest. Additionally, a comparison of these experimental results with the results in the slumped configuration will be of interest.

3. Small Sample Reactivity Worths in Reference Core

Table V lists the reactivity worths of the important samples measured at the center of the reference core. These numbers represent composite sample worths and isotopic corrections are needed to obtain the individual isotopic worths. The results shown are consistent with results obtained in earlier assemblies. Once again, the primary interest in these parameters is in the ability of standard calculational methods to predict the magnitudes of these parameters. Axial reactivity worths profiles of ^{239}Pu, ^{238}U and stainless steel were also measured.

4. Prompt Neutron Lifetime (ℓ) Measurement

Measurements were made of the β/ℓ of the reference assembly and the axially symmetric fuel slump-in configuration using reactor noise analysis

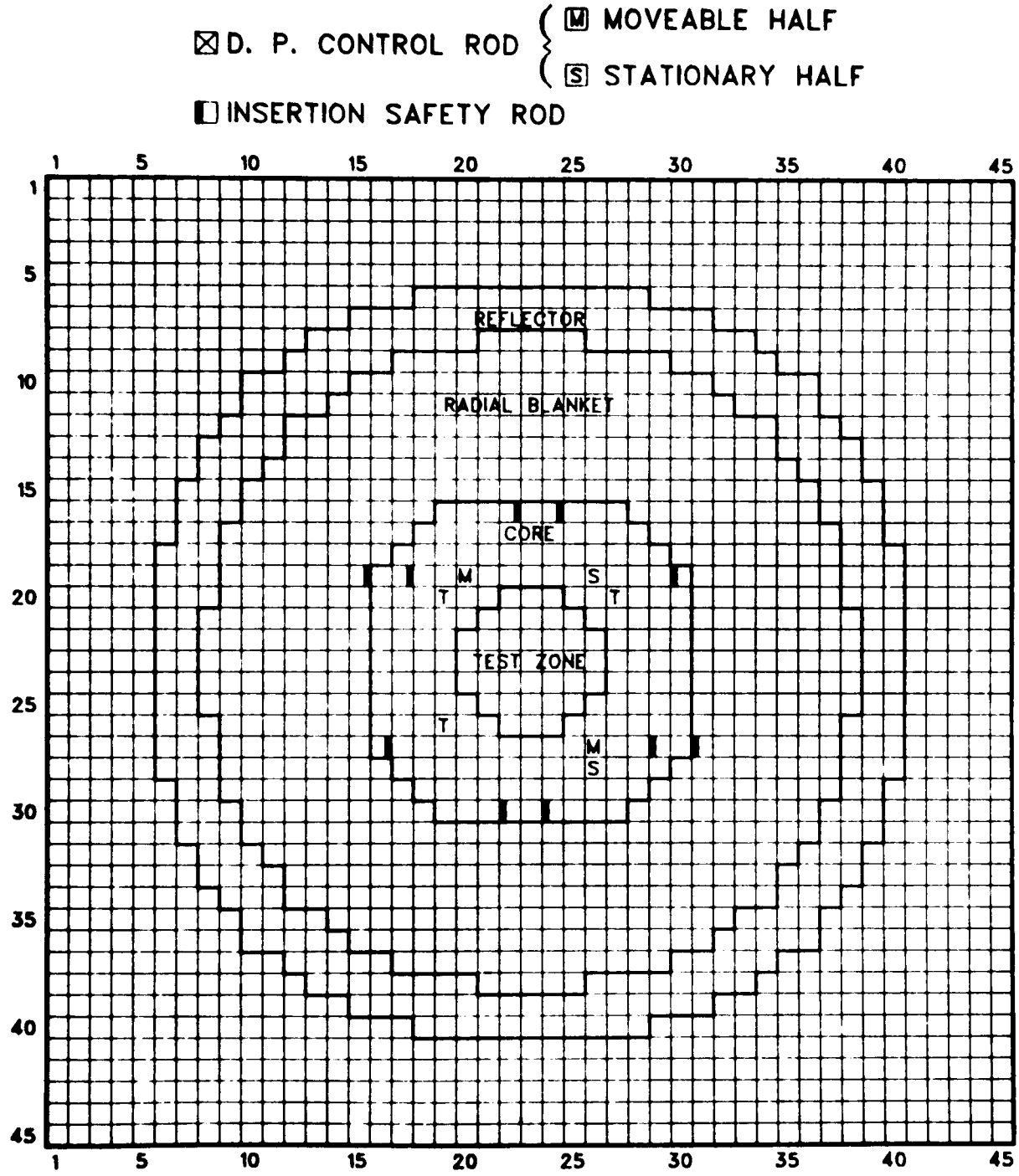

Fig. 2. Core Layout of the Reference Assembly. ANL Neg. No. 116-78-125

TABLE III. Enriched Uranium Fission Rates in the RSR Reference Configuration, Radial Packet Locations

Drawer[2]	Relative Enriched Uranium Fission Rate[1]			
	Z = 1 in.	Z = 3 in.	Z = 5 in.	Z = 7 in.
M22/24	985.8 ± 3.9	971.2 ± 4.8	947.6 ± 3.9	905.9 ± 4.0
M23/24	995.2 ± 5.2	983.9 ± 3.8	952.6 ± 3.8	900.2 ± 4.4
M24/24	981.5 ± 2.7	970.4 ± 3.2	936.2 ± 3.3	895.4 ± 2.5
S22/26	905.2 ± 3.7	904.2 ± 3.2	891.0 ± 3.5	832.8 ± 3.5
S23/26	914.6 ± 4.0	902.6 ± 3.8	877.6 ± 3.5	838.4 ± 3.4
S24/26	904.3 ± 4.1	888.1 ± 4.4	870.4 ± 3.7	828.5 ± 3.0
M22/26	901.9 ± 4.3	885.8 ± 4.1	862.4 ± 4.1	824.7 ± 4.0
M23/26	916.2 ± 3.4	899.2 ± 3.4	868.0 ± 3.4	832.2 ± 3.4
M24/26	898.7 ± 5.6	884.6 ± 4.7	855.4 ± 4.6	817.6 ± 4.4
S22/28	757.4 ± 4.6	738.2 ± 2.6	732.6 ± 3.3	692.4 ± 4.3
S23/28	764.0 ± 2.7	747.8 ± 2.9	752.2 ± 3.2	713.2 ± 2.6
S24/28	749.9 ± 3.2	742.4 ± 2.8	725.2 ± 2.8	692.1 ± 3.2
M22/28	758.4 ± 3.2	733.5 ± 4.1	717.4 ± 2.8	690.9 ± 4.2
M23/28	765.5 ± 4.1	753.6 ± 3.6	724.7 ± 3.1	690.7 ± 3.2
M24/28	745.8 ± 4.2	737.6 ± 3.2	717.0 ± 3.2	686.0 ± 2.9
S22/30	589.1 ± 2.6	573.5 ± 2.4	563.1 ± 2.1	537.6 ± 2.5
S23/30	588.3 ± 2.6	583.3 ± 2.6	565.3 ± 2.6	541.5 ± 2.4
S24/30	579.9 ± 2.8	568.2 ± 2.2	554.7 ± 2.7	530.3 ± 2.8
S22/31	526.1 ± 2.6	512.4 ± 3.2	501.5 ± 3.1	473.9 ± 2.9
S23/31	523.6 ± 2.3	518.4 ± 3.0	502.9 ± 2.5	477.6 ± 2.7
S24/31	521.4 ± 2.8	513.6 ± 2.5	501.0 ± 1.8	479.4 ± 2.1
M22/31	518.3 ± 2.1	513.3 ± 2.1	500.7 ± 2.3	481.8 ± 2.0
M23/31	529.1 ± 2.3	520.4 ± 2.5	506.3 ± 2.8	480.4 ± 2.9
M24/31	527.0 ± 2.3	521.6 ± 2.6	501.5 ± 1.9	482.9 ± 2.0
S22/34	323.0 ± 1.1	314.4 ± 1.0	306.4 ± 1.4	291.3 ± 2.3
S23/34	323.1 ± 2.0	316.8 ± 2.3	309.2 ± 1.7	295.9 ± 1.4
S24/34	315.2 ± 4.3	314.0 ± 1.6	302.6 ± 1.3	290.0 ± 1.6
M22/34	322.5 ± 1.6	313.1 ± 2.3	310.5 ± 1.9	259.8 ± 7.0
M23/34	320.2 ± 1.5	316.9 ± 1.7	308.3 ± 1.7	297.0 ± 1.1
M24/34	317.0 ± 2.5	314.1 ± 2.1	304.8 ± 2.2	291.8 ± 1.4

[1]Errors listed are relative statistical counting undertainties only.
[2]Drawer identification 22/24 refers to row 22, column 24; M and S refer to movable and stationary (axial) halfs of the reactor respectively.

TABLE IV. Enriched Uranium Fission Rates in the RSR Reference Configuration, Axial Packet Locations

Z (IN.)	Relative Enriched Uranium Fission Rate[1]				
	S21/24[2]	S22/24	S23/24	S24/24	S25/24
1.00	962.3 ± 4.4	983.4 ± 5.6	997.6 ± 5.5	975.2 ± 6.9	950.2 ± 5.2
3.00	941.0 ± 5.0	968.8 ± 4.7	980.3 ± 4.9	970.7 ± 5.5	942.3 ± 4.6
5.00	915.6 ± 5.3	941.2 ± 6.0	953.4 ± 4.4	932.2 ± 4.8	910.0 ± 4.1
7.00	871.4 ± 5.4	893.8 ± 4.4	907.4 ± 5.8	903.7 ± 4.3	866.9 ± 4.0
9.00	822.4 ± 4.0	844.4 ± 5.1	846.1 ± 4.6	837.9 ± 3.7	819.3 ± 4.0
11.00	755.4 ± 3.9	766.6 ± 3.7	782.1 ± 4.7	765.0 ± 4.2	758.5 ± 2.3
12.75	692.6 ± 3.5	713.7 ± 4.6	715.2 ± 4.0	716.2 ± 4.2	699.5 ± 3.8
14.25	638.1 ± 2.8	654.5 ± 6.1	667.2 ± 3.8	640.3 ± 5.9	635.6 ± 3.7
15.75	582.4 ± 3.1	595.4 ± 2.7	606.9 ± 3.4	601.6 ± 2.9	581.2 ± 3.0
17.25	529.0 ± 2.8	540.7 ± 2.8	551.6 ± 3.8	546.0 ± 3.7	532.5 ± 1.6
18.75	494.9 ± 2.1	507.9 ± 2.9	519.0 ± 3.2	520.6 ± 2.0	495.4 ± 3.6
20.25	451.7 ± 2.0	467.4 ± 2.5	472.3 ± 3.2	476.7 ± 2.7	451.1 ± 3.4
21.75	416.0 ± 2.6	423.6 ± 2.5	428.3 ± 2.5	431.1 ± 2.2	416.7 ± 2.1
23.25	369.0 ± 2.2	377.7 ± 2.1	377.1 ± 2.0	383.4 ± 2.1	375.4 ± 2.1
24.75	322.3 ± 1.6	331.2 ± 1.8	337.9 ± 1.9	341.0 ± 1.8	329.0 ± 2.1
26.25	275.8 ± 1.4	288.8 ± 2.2	287.0 ± 1.7	294.3 ± 1.4	281.6 ± 1.4
27.75	233.0 ± 1.5	237.6 ± 1.6	242.6 ± 1.5	247.1 ± 1.1	235.1 ± 1.5
29.25	192.8 ± 1.2	199.4 ± 1.2	199.9 ± 1.1	202.7 ± 1.4	192.2 ± 1.3

[1]Errors listed are relative statistical counting uncertainties only.
[2]Drawer identification 21/24 refers to row 21, column 24; the S refers to the stationary half of the reactor.

TABLE V. Results of Small-Sample Reactivity Worth Measurements in the Reference Assembly

Sample I.D.	Major Isotope/ Element/Compound in Sample	Central Reactivity Worth (Ih/kg)
MB-10	^{239}Pu	374 ± 4
Pu-240-2	$^{240}PuO_2$	97 ± 1
MB-21	^{235}U	250 ± 3
MB-25	^{238}U	-17.6 ± 0.7
B-7	^{10}B	-5470 ± 90
MB-19	Stainless Steel	-10.5 ± 0.2
NA (1.2)	Na	-8.7 ± 1.7

methods. Specifically, two detectors were placed in the assemblies and random components of their outputs were analyzed to obtain the cross-spectra. This was fit to the expression $A/(\alpha^2 + \omega^2)$ to obtain $\alpha = \beta/\ell$.

Two measurements were made in the reference assembly (one with the reactor cooling fans on and the other with the cooling fans off) and one measurement was made in the fuel slump-in configuration (with cooling fans turned off). This was done to check whether the detectors were picking up microphonic noise from the cooling fans. The data from each run, corrected for calibration, were fitted to the expression for the expected spectrum by variable metric minimization. The results of the fitting are shown in Figs. 3, 4 and 5. It appears that the variable metric is not finding the best fit, so alternative fitting methods are being explored. Table VI lists the resulting values of β/ℓ from these fits and the preanalysis calculated values. Because of the nature of the fits, the experimental numbers should be treated as preliminary. No estimate of the precision is available at this time. The calculated predictions of the β/ℓ parameter are also presented in Table VI. It is noted that a considerable improvement in the C/E ratio occurs in going from the preanalysis to the post analysis - the difference being attributable mainly to the improved cross sections. Additionally, the calculated prediction for the slump-in configuration is considerably worse than for the reference configuration.

Status of the Diffusion Theory Analysis

The progress of the diffusion theory analysis of the experiments was impeded for several months by cross-section processing code problems. These problems have recently been corrected and the anlaysis is proceeding smoothly. Isotopic cross-sections have been generated for all the compositions encountered in the program. Benoist bi-directional diffusion coefficients were also generated for all the compositions for use in the two-dimensional diffusion theory analysis.

It has been determined that for the core regions for neutron energies above ~2 keV, the neutron streaming process is better described using Gelbard diffusion coefficients[9] instead of Benoist diffusion coefficients. Gelbard diffusion coefficients have been generated for the normal core, sodium voided core and slumped core configurations.

An R-Z calculational model of the reference core has been set up (Fig. 6) and an eigenvalue calculation has been performed. The final eigenvalue of 0.9903 is quite close to earlier calculational experience with critical assemblies. Table VII summarizes the basic results.

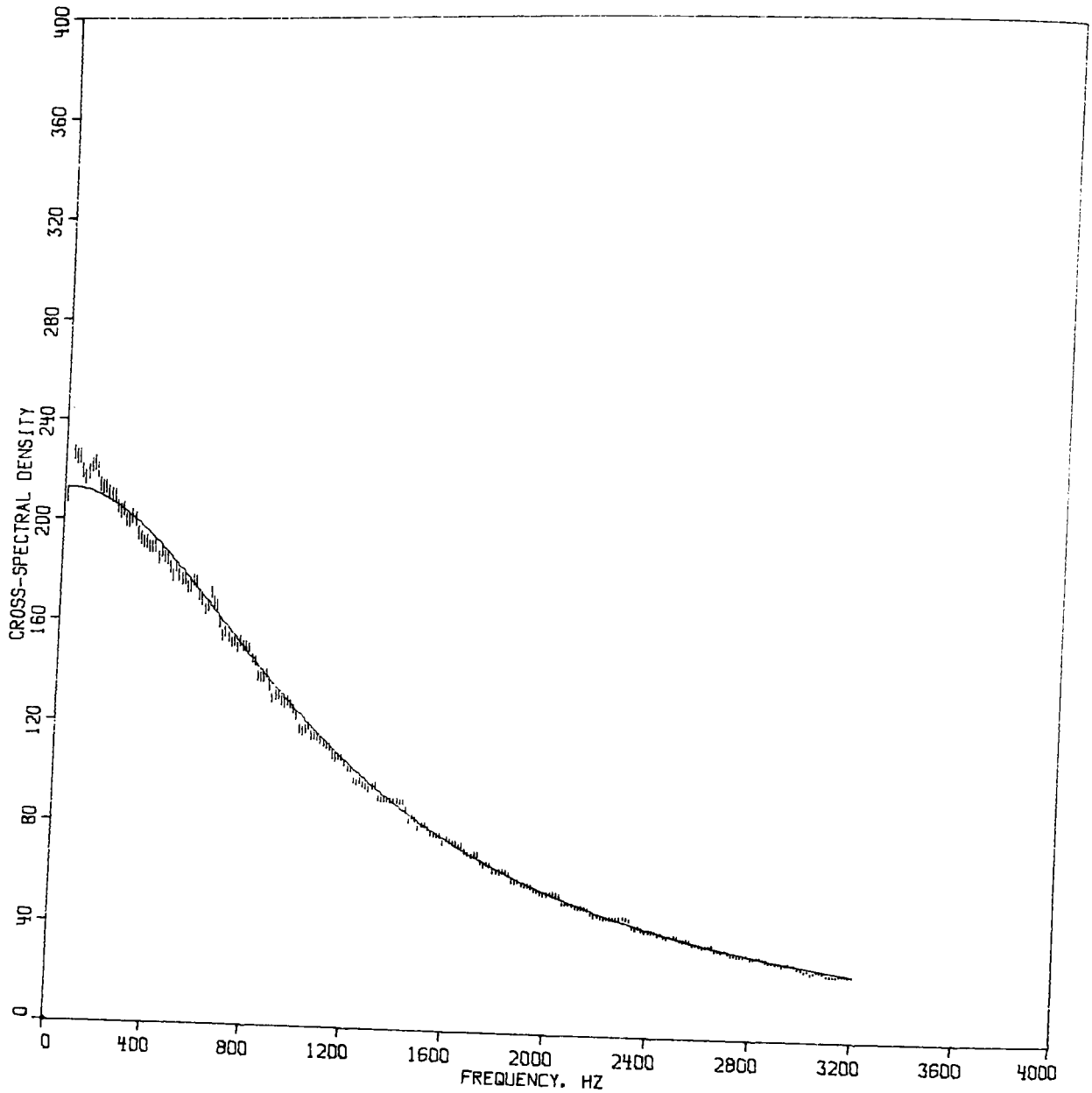

Fig. 3. Noise Spectrum Data for the Reference Core with Reactor Cooling Fans On. ANL Neg. No. 116-78-128

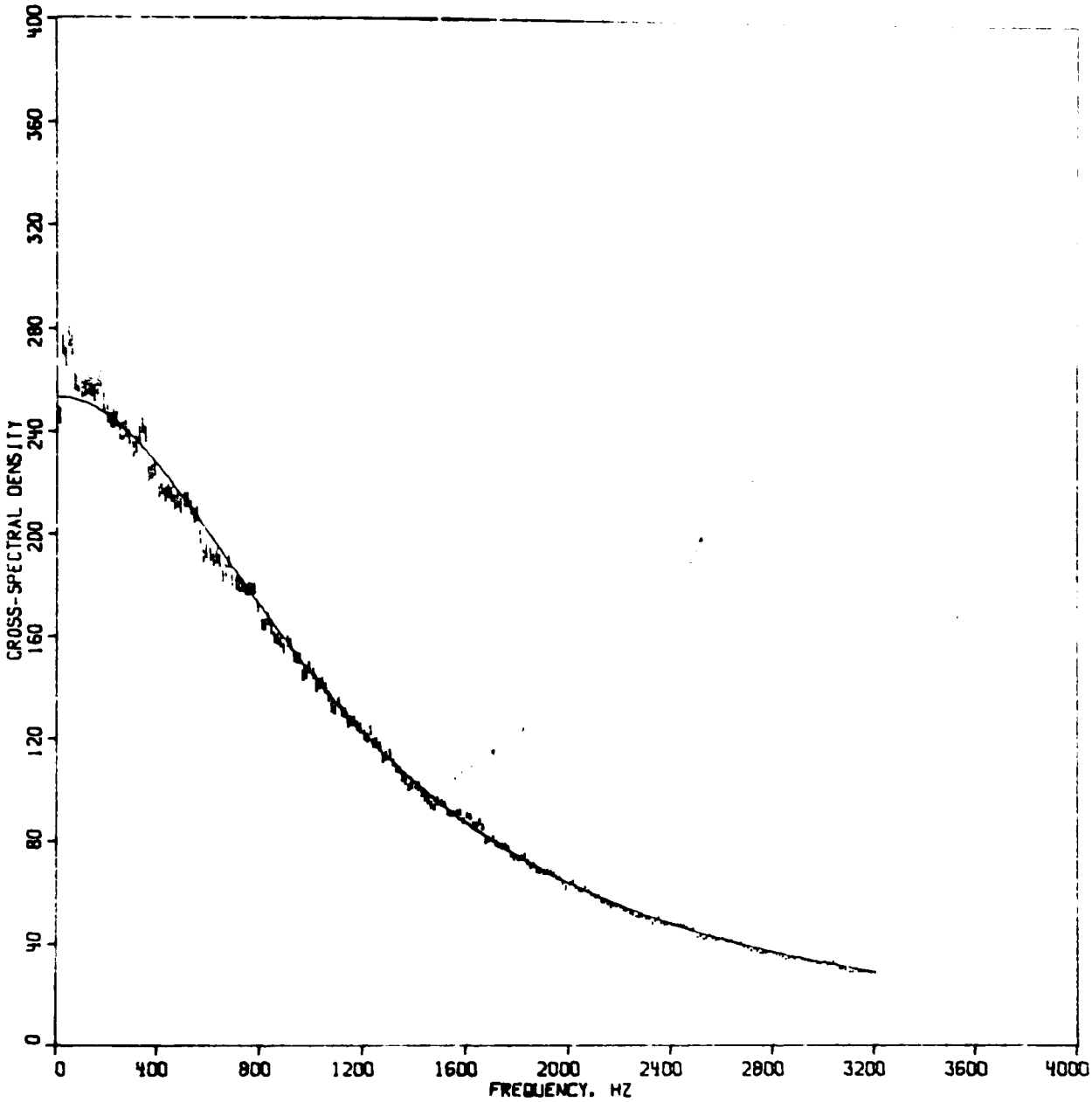

Fig. 4. Noise Spectrum Data for the Reference Core with Reactor Cooling Fans Off. ANL Neg. No. 116-78-129

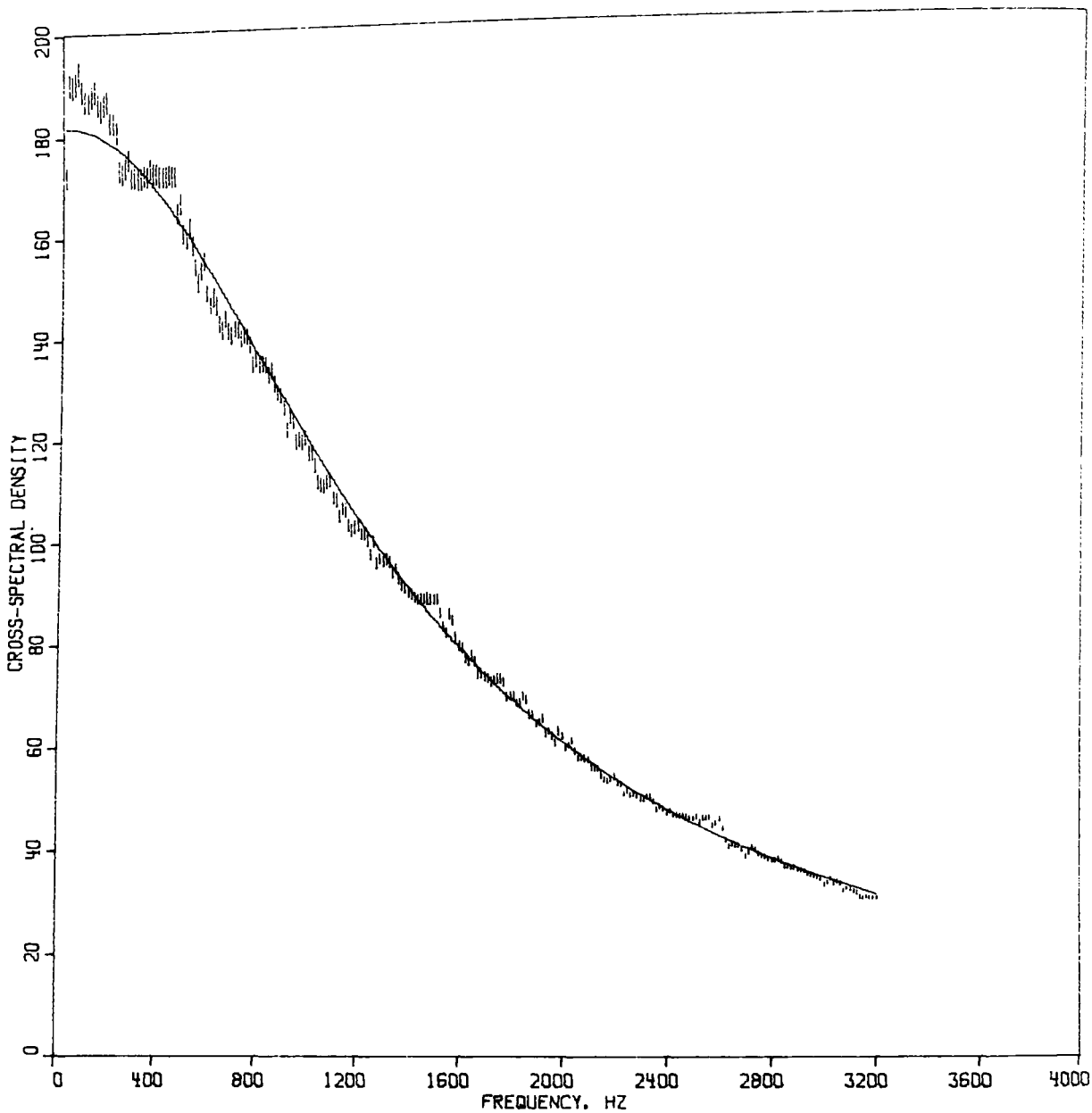

Fig. 5. Noise Spectrum Data for the Fuel Slump-In Core with Reactor Cooling Fans Off. ANL Neg. No. 116-78-130

TABLE VI. Preliminary Results of β/ℓ Measurements in the Reference and Fuel Slump-In Configurations

Configuration	β/ℓ, sec^{-1}				
		Preanalysis		Post Analysis	
	Experimental	Calculated Value	C/E	Calculated Value	C/E
Reference[a]	7305	9731	1.33	8532	1.168
Reference[b]	7350	9731	1.34	8532	1.161
Fuel Slump-In[b]	8554	13909	1.63	10542	1.238

[a]With reactor cooling fans on.

[b]With reactor cooling fans off to avoid the pickup of microphonic noise.

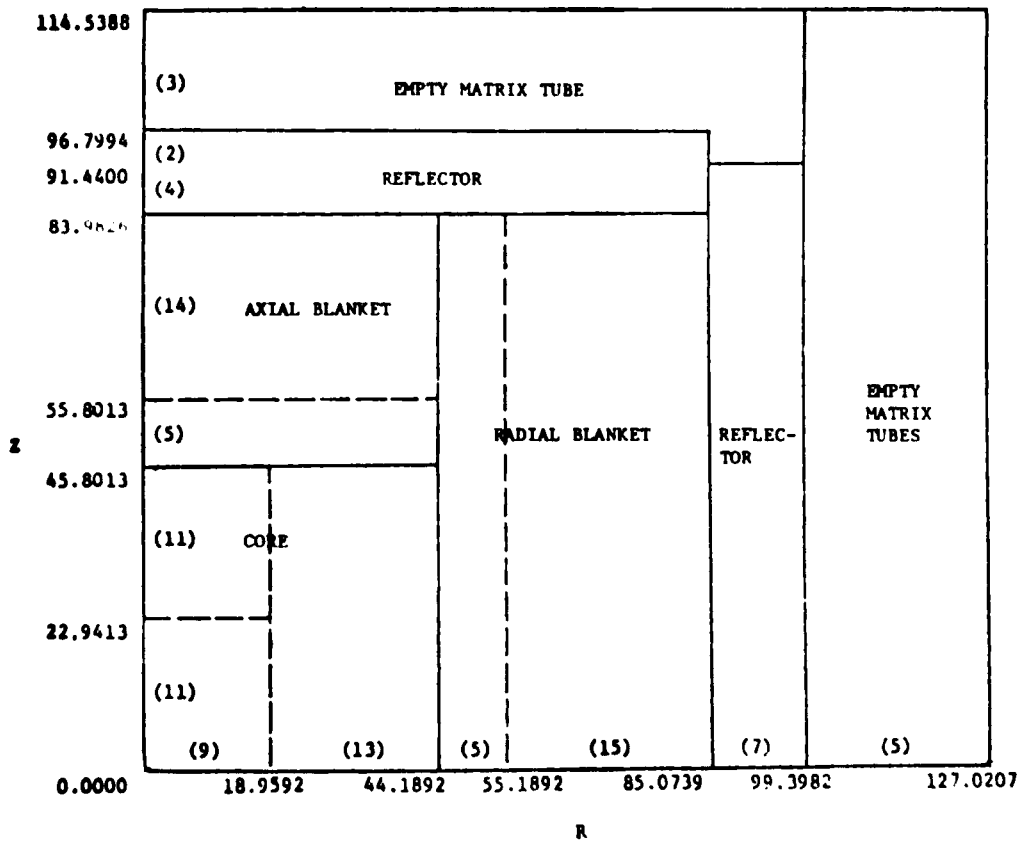

Regions and compositions are indicated by solid lines; cross-section types are indicated by dashed lines. The number of mesh intervals is shown in parentheses. All dimensions are in centimeters.

Fig. 6. The R-Z Model of the Reference Assembly. ANL Neg. No. 116-78-127

TABLE VII. Results of Diffusion Theory Analysis for Reference Core

Parameter	Calculated Value
1. Eigenvalue of reference configuration[a]	0.9903
2. δk for streaming	-0.0029
3. δk for transport correction	+0.0012
4. Percent of total fissions in test zone (relative to total fissions in assemblies)	23.78 %
5. Percent of total absorptions in zone (relative to total absorptions in assembly)	14.32%
6. K_∞ of test zone	1.69

[a] This includes the effects of streaming and transport listed in items 2 and 3.

III. THREE-DIMENSIONAL CODE DEVELOPMENT FOR CORE THERMAL HYDRAULIC ANALYSIS OF LMFBR ACCIDENTS UNDER NATURAL CONVECTION CONDITIONS (A2045)

A. Initial and Boundary Conditions (W. T. Sha and H. M. Domanus)

Initial and boundary conditions available in COMMIX-1 are presented below:

1. Initial Conditions

Generally, before the solution sequence can begin all variable values must be assigned. This is accomplished by either continuing a previous run, via the restart capability, or by specifying the initial temperature (T), pressure (P), and velocity (u,v,w) distribution throughout the interior points of the configuration under consideration. When the initialization is not a restart, density (ρ) and enthalpy (h) are calculated from equations of state using the specified pressures and temperatures. Because determination of these distributions and their subsequent input into the code can be tedious, certain options have been provided to ease the initialization task. When a steady-state solution is being sought, an initialization as close as possible to the expected solution should be used to reduce computer running time.

2. Pressure Initialization for Static Head

When gravity is acting along any of the three principle axes and there is either constant or one dimensional temperature variation in that same direction, an option is available to reduce the initialization task. This is accomplished by specifying a pressure at a point and the constant or one-dimensional temperature variation. The entire temperature field is generated from the input temperature information. The density field is computed by the equation of state. Using this density field and the point pressure, a pressure field is generated to account for the static head. From the pressure and temperature fields, the enthalpy is obtained, thus completing this initialization option.

3. Pressure Drop Initialization

A linear variation or constant pressure gradient initialization option is available in COMMIX-1. This can be used when the constant pressure gradient is along any one of the three principle axes. It is accomplished by specifying the constant pressure gradient as either,

$$\frac{\partial P}{\partial x}, \frac{\partial P}{\partial y}, \text{ or } \frac{\partial P}{\partial z}$$

and a point pressure. This option can be used along with the static head initialization. However, if the constant pressure gradient is along the same axis as gravity, the pressure gradient due to gravity must be included in the specification of the constant pressure gradient.

4. One Dimensional Initialization for Hexagonal Fuel Assemblies

If a hexagonal fuel assembly calculation is being performed, the z-axis is aligned with the axial length. If gravity is acting along the z-axis and the inlet is from the z = 0 plane, a one dimensional initialization option is available. The initialization is performed assuming transverse velocities are zero and all variables constant throughout a given axial (z = constant) plane. This initialization takes into account drag and static head forces as well as internal heat sources. This option has proved to reduce the computer running time to reach steady-state solution for hexagonal fuel assemblies.

5. Boundary Conditions

Each surface bounding the configuration has two boundary conditions associated with it, one on velocity and the other for temperature. Each of these boundary conditions are treated separately so that any combination of velocity and temperature boundary conditions can be associated with the surface.

6. Velocity Boundary Conditions

There are five (5) velocity boundary conditions available in COMMIX-1 All inlet and outlet boundary conditions assume parallel flow. The first is where the boundary normal velocity $(V_b)_n$ is set initially and remains unchanged throughout the solution, i.e.,

$$(V_b)_n = C \text{ (constant velocity).}$$

A no slip surface may be specified by setting $(V_b)_n = 0$. An inlet is specified by a +C and an outlet indicated by a -C.

The second velocity boundary condition is the uniform transient. For this boundary conditions the boundary normal velocity is set equal to a transient function f(t) at the beginning of every timestep, i.e.,

$$(V_b)_n = f(t) \quad \text{(transient velocity).}$$

When f(t) has positive values it is an inlet, while when f(t) has negative values it is an outlet.

The third boundary condition is the free slip wall. With this boundary condition the boundary normal velocity is set equal to zero, while the boundary tangent velocity, $(V_b)_t$, is set equal to its corresponding adjacent internal velocity $(V_i)_t$ so that the wall shear stress, τ_b, is zero, i.e.,

$$(V_b)_n = 0$$

$$(V_v)_t = (V_i)_t \quad \text{(free slip wall)}$$

and $\tau_b = 0.$

The fourth and fifth boundary conditions are outlet boundary conditions used to minimize the upstream influence of the outlet. These are the continuative velocity outlet and the continuative momentum outlet. The continuative velocity outlet has the boundary normal velocity set equal to the corresponding adjacent internal velocity, i.e.,

$$(V_b)_n = (V_i)_n \quad \text{(continuative velocity outlet).}$$

The continuative momentum velocity outlet sets the boundary normal velocity such that the boundary normal momentum is equal to the corresponding adjacent internal momentum, i.e.,

$$(V_b)_n = \frac{\rho_i (V_i)_n}{\rho_b} \quad \text{(comtinuative momentum outlet).}$$

where ρ_b, ρ_i = densities at the boundary and of its adjacent internal cell, respectively.

7. Temperature Boundary Conditions

There are five (5) temperature boundary conditions available in COMMIX-1. These are the uniform constant temperature, uniform transient temperature, uniform constant normal heat flux, uniform transient normal heat flux and the adiabatic boundary conditions. For each of these boundary conditions, density and enthalpy are assigned from equations of state after the boundary temperature has been determined.

The uniform constant temperature boundary condition sets the boundary temperature, T_b, initially and remains unchanged throughout the solution, i.e., $T_b = C$.

The conduction length $(VX)_c$ is given in terms of the surface area A_b and the volume of the adjacent internal $(VOL)_i$ as

$$(VX)_c = \frac{(VOL)_i}{A_b} .$$

The normal heat flux, $(q_b)_n$, is computed from the temperature at the adjacent internal cell, T_i, i.e.,

$$(q_b)_n = k(T_b)\frac{(T_b - T_i)}{(\nabla X)_c} \text{(constant temperature)},$$

where k = thermal conductivity.

The uniform transient temperature boundary condition is performed by setting the boundary temperature equal to a transient function, f(t), i.e.

$$T_b = f(t)$$

and

$$(q_b)_n = k(T_b)\frac{(T_b - T_i)}{(\nabla X)_c} \quad \text{(transient temperature)}.$$

The uniform constant normal heat flux boundary condition sets the normal heat flux at the boundary initially and is unchanged throughout the solution. The boundary temperature is computed from the temperature of the adjacent internal cell. Positive heat flux values indicate heat is being added to the configuration, while negative values indicate heat loss, i.e.

$$(q_b)_n = C$$

and

$$T_b = T_i + \frac{(q_b)_n (\nabla X)_c}{k(T_b)} \text{ (constant heat flux)}.$$

The uniform transient normal heat flux boundary condition assigns a transient function, f(t), to the boundary normal heat flux as

$$(q_b)_n = f(t)$$

where

$$T_b = T_i + \frac{(q_b)_n (\nabla X)_c}{k(T_b)} \text{ (transient heat flux)}.$$

The adiabatic boundary conditions initially sets the boundary normal heat flux to zero and the boundary temperature equal to the adjacent internal cell temperature during solution, i.e.,

$$(q_b)_n = 0.$$

and

$$T_b = T_i \quad \text{(adiabatic)}.$$

References

1. C. R. Bell, P. J. Blewett, J. E. Boudreau and J. L. Tompkins, "Investigation of Postdisassembly Core Expansion Energetics," Nuclear Reactor Safety, Quarterly Progress Report for the Period of July-September 1977, Los Alamos Scientific Laboratory, pp. 24-28.

2. M. A. Grolmes, G. A. Lambert and H. K. Fauske, "Liquid Film Thickness for a Single-Bubble Slug Ejection," Trans. Am. Nucl. Soc., 14(1), pp. 242-243 (June 1971).

3. D. H. Cho, M. Epstein and H. K. Fauske, "Work Potential Resulting from a Voided-Core Disassembly," Trans. Am. Nucl. Soc., 18, p. 220 (June 1974).

4. P. L. Garner, "Condensation of Fuel onto the Above-Core Structure During an LMFBR Core-Disruptive Accident," NUREG-0344, University of Virginia (October 1977).

5. A. Suo-Antilla, "Multicomponent Vapor-Liquid Phase Transition Model," Nuclear Reactor Safety, Quarterly Progress Report for the Period of January-March 1977, LA-NUREG-6842-PR, Los Alamos Scientific Laboratory, pp. 46-49 (June 1977).

6. H. Zimmermann, "Fission Gas Behavior in Oxide Fuel Elements of Fast Breeder Reactors," Nucl. Techl., 28, pp. 127-133 (January 1976).

7. S. K. Bhattacharyya, private communication (1977).

8. H. Ludewig, "Preliminary Analysis of the Proposed BIZET-B Safety Related Critical Experiments," BNL-NUREG 23006, Brookhaven National Laboratory (June 1977).

9. E. M. Gelbard et al., "Calculations of Void Streaming in the Argonne Gas-Cooled Fast Reactor Critical Experiments," Nucl. Sci. Eng. 64(2), 624 (1977).